DYNAMIC FRICTION BEHAVIOR IN PRE-SLIDING REGIME OF PNEUMATIC ACTUATORS

Tran Xuan Bo[1*], Do Viet Long[1], and Hideki Yanada[2]

[1]Department of Fluid Power & Automation Engineering, School of Transportation Engineering, Hanoi University of Science and Technology, Hanoi, Vietnam, e-mail: bo.tranxuan@hust.edu.vn

[2]Department of Mechanical Engineering, Toyohashi University of Technology, Toyohashi, Japan, e-mail: yanada@me.tut.ac.jp

Received Date: February 6, 2017

Abstract

This paper focuses on investigating friction behavior in pre-sliding regime and developing a new mathematical model of friction for fluid power actuators. Using pneumatic cylinders with different sizes, an experimental setup is built to measure friction force-displacement characteristics in pre-sliding regime under various conditions of pressures in the cylinder chambers. A new mathematical model of friction for the pneumatic cylinders is proposed by incorporating a hysteresis function into the new modified LuGre model. The experimental results show that when the pressures are varied, friction of the pneumatic cylinders in pre-sliding regime is represented by behavior of a nonlinear spring. In addition, hysteresis behavior with nonlocal memory is obtained in the friction force-displacement characteristics and that the size of the hysteresis loop is increased with increasing pressures in the cylinder chambers. The simulation results show that the new friction model can accurately simulate the friction behavior of the pneumatic cylinders in pre-sliding regime as well as sliding regime.

Keywords: Fluid Power Actuator, Friction Behavior, Friction Model, Pneumatic Cylinder, Pre-sliding

Introduction

Fluid power actuators are widely used in applications that require high power and high stiffness such as construction machines, material pressing machines, industrial robots, etc. However, friction is always present in the fluid power actuators and significantly affects the performances of the fluid power actuator systems. Friction can cause power reduction, stick-slip motion, and difficulties in controlling the systems. Therefore, fully understanding of the behavior of friction and developing an adequate mathematical model of friction for the fluid power actuators is very necessary in designing and controlling them.

Many works have been done to deal with these tasks. The references [1-4] experimentally examined friction force-velocity or friction torque - rotational speed characteristics and developed mathematical models of friction for both hydraulic and pneumatic actuators. However, these works focused only on the friction behavior under steady-state conditions, i.e. at constant velocities.

For oscillating velocity conditions, Nouri [5] proposed an experimental test setup to identify the friction force in both pre-sliding regime (i.e. in the regime that velocity is very near zero) and sliding regime of a rodless pneumatic cylinder. He observed hysteresis behavior in both friction force-piston displacement and friction force-velocity characteristics. Yanada and Sekikawa [6] examined dynamic friction behavior of a hydraulic cylinder under sinusoidally varying velocity conditions. They showed that when the velocity varies with velocity reversal, the friction force lags behind the velocity and that the maximum friction

force reduces after the first cycle of the velocity variation. In order to capture such behavior, they proposed a friction model for the hydraulic cylinder. This model was developed from the LuGre model [7] by adding a lubricant film dynamics into the LuGre model and was called the modified LuGre model. The validity of the modified LuGre model was verified by the measured dynamic friction behavior of hydraulic cylinders under various conditions of piston velocity using different hydraulic oils [6, 8]. However, Tran et al. [9] showed that the modified LuGre model is valid only in negative resistance regime, i.e., in the velocity range that friction force reduces with increasing velocity and that it cannot simulate the hysteretic behavior observed in the hydraulic cylinders in fluid lubrication regime. They revised the modified LuGre model by replacing the usual fluid friction term with a first-order lead dynamics and showed the usefulness of the new modified LuGre model in the entire sliding regime.

Recently, Tran and Yanada [10] measured dynamic friction behavior of pneumatic cylinders under various conditions of velocity and pressures in the cylinder chambers. They showed that hysteretic behavior can be seen at low velocities in the friction force-velocity relation and the friction force varies nearly linearly with the velocity at high velocities. Size of the hysteretic loop is increased with increasing driving pressure and is decreased with increasing resistance pressure. They also reported that such friction behavior of the pneumatic cylinders can be accurately simulated by the new modified LuGre model by expressing some parameters as functions of frequency of velocity variation, though the model becomes complicated.

As mentioned above, the dynamic friction behavior of fluid power actuators has been examined and modeled but have not fully been done. For instance, the dynamic friction behavior of asymmetric hydraulic or pneumatic cylinders in pre-sliding regime under different conditions of pressures in the cylinder chambers has not been examined. Therefore, in this paper an experimental setup is proposed to examine friction behavior in pre-sliding regime of pneumatic cylinders under different conditions of pressures. Limitation of the new modified LuGre model in simulating the measured results is pointed out and then a new mathematical model of friction for the pneumatic cylinders is proposed. The usefulness of the new mathematical model is confirmed by the comparisons with experimental results.

Experimental System

The experimental system used in this investigation is shown in Figure 1. In this system, a pneumatic cylinder was fixed horizontally on a flat base and the piston head was directly connected by a threaded joint to a cylindrical object made of iron. The piston and the object were freely moved without a guiding. Two proportional pressure control valves with a rated pressure of 1 MPa were used to control the pressures in the chambers of the pneumatic cylinder. The input current of the valves ranges from 0 to 1 A. An eddy current type displacement sensor with a measuring range of 2 mm and a full scale accuracy less than 0.5 % was used to measure the displacement x of the piston. Two pressure sensors with a rated pressure of 1 MPa and a full scale accuracy less than 1 % were used to measure the pressures p_1 and p_2 in the cylinder chambers. The voltage signals from the displacement sensor and the pressure sensors were read by a personal computer through an analog to digital converter (ADC) and the computer supplies two control signals to the proportional valves through a digital to analog converter (DAC). Two amplifiers were used to operate the two proportional pressure control valves. The input voltage of the amplifiers ranges from 0 to 5 V. The program for data acquisition was made using Microsoft visual C++ software. The pressures, p_1, p_2, and the piston displacement, x, were recorded at the interval of 1,1 ms. A photo of the experimental system is shown in Figure 2.

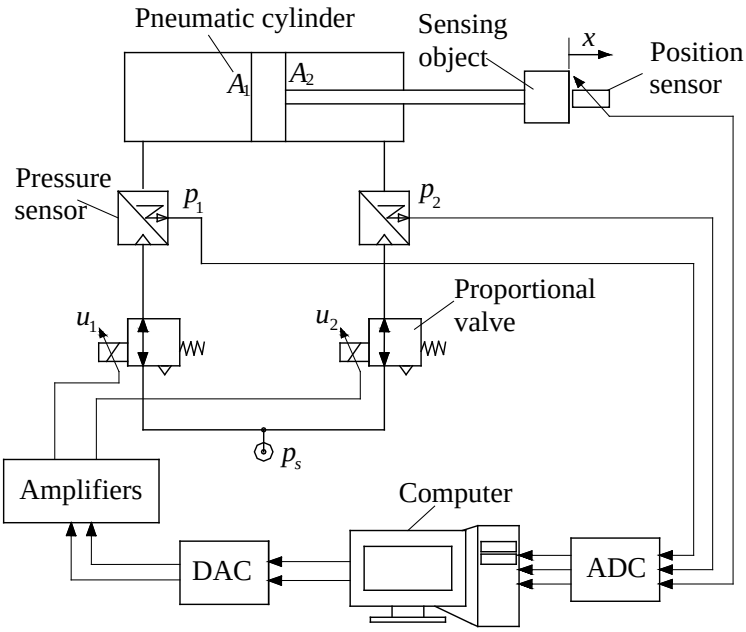

Figure 1. Schematic diagram of the experimental system

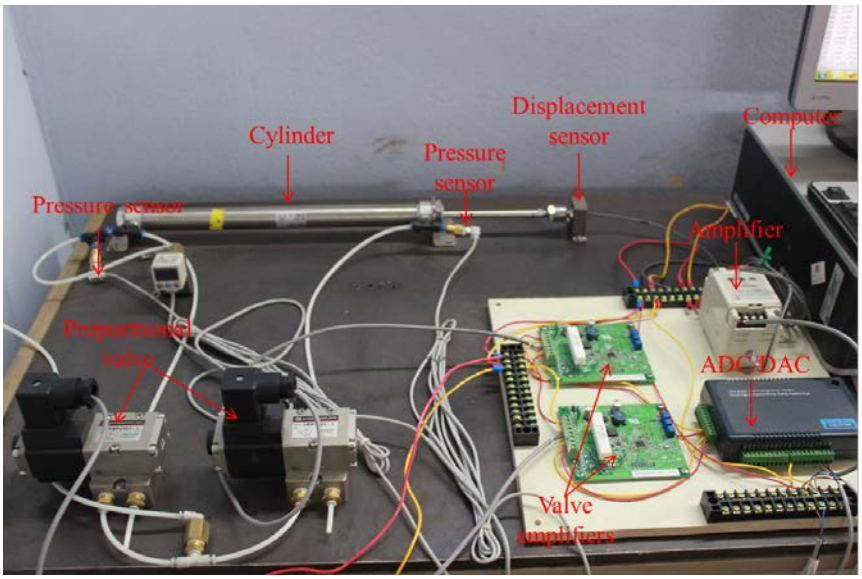

Figure 2. Photo of the experimental system

The friction force F_r was calculated by the equation of motion of the piston from the measured values of the pressures, p_1 and p_2, and the acceleration, a, as follows:

$$F_r = p_1 A_1 - p_2 A_2 - ma \tag{1}$$

where A_1, A_2 are the pressure receiving areas; m is the total mass of the piston, piston rod and the sensing object. The acceleration was approximately calculated by a second order differentiation of the measured piston displacement. The noise in the calculated acceleration signal was filtered by a first-order acausal low-pass filter with a bandwidth of 10 Hz.

Three pneumatic cylinders with different sizes shown in Table 1 were used to investigate the friction behavior in pre-sliding regime under different pressures in the two

cylinder chambers. To vary the pressures, the square pulse signals u_1 and u_2 with magnitude varying from 0 to 5 V were supplied to the proportional pressure control valves. The supply pressure p_s was set in the range of 0.1 to 0.6 MPa. Figure 3 shows an example of the measured variables p_1, p_2, x and the calculated friction force F_r when u_1 and u_2 are given as shown in Figure 3a for Cylinder 1 at p_s=0.5 MPa.

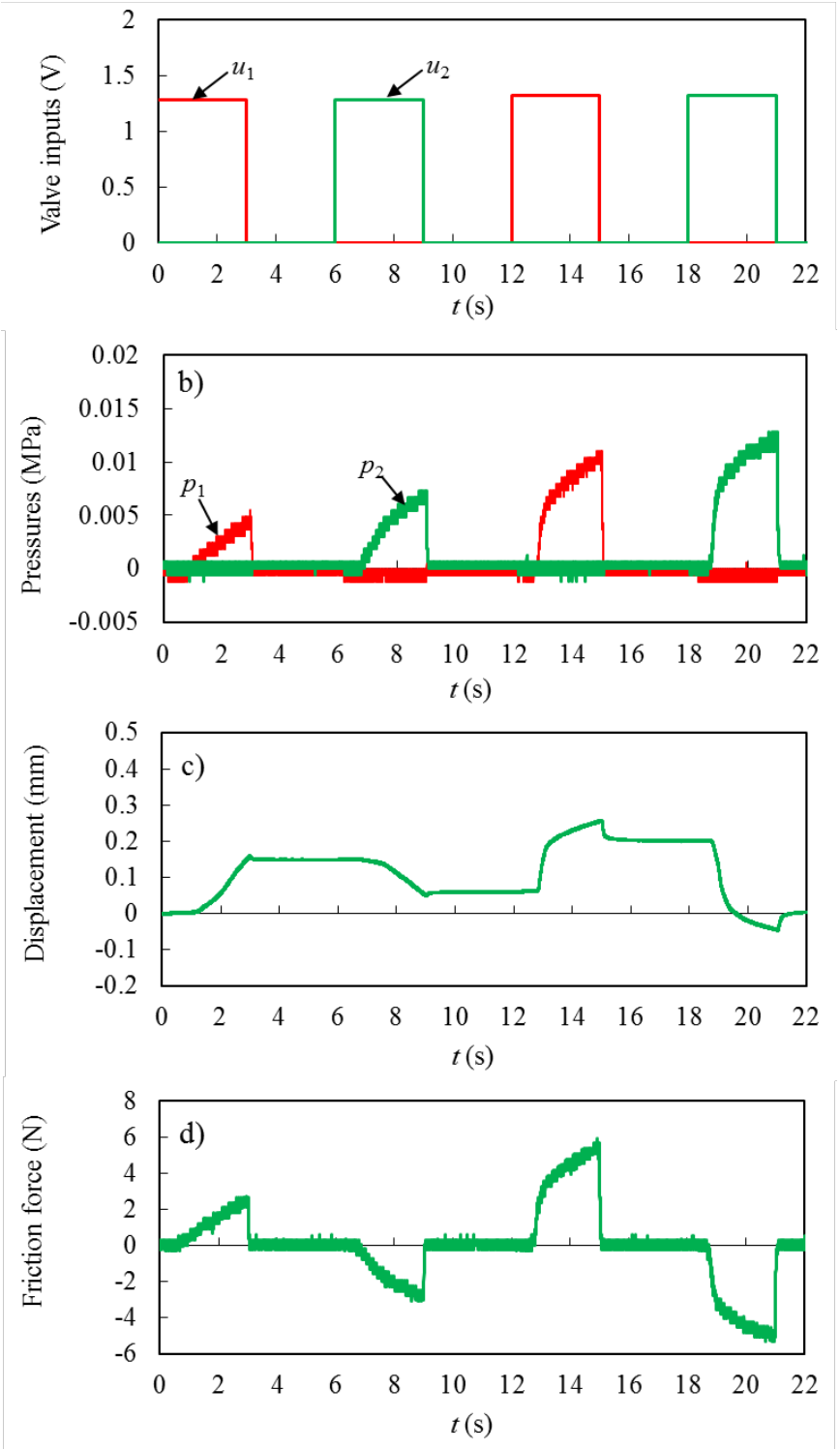

Figure 3. Example of experimental data of Cylinder 1 at p_s=0.5 MPa: (a) valve inputs, (b) variation of pressures p_1 and p_2, (c) variation of piston displacement x, (d) variation of friction force

Table 1. Dimensions of Pneumatic Cylinders Used

Cylinder	Bore Dia. (mm)	Rod Dia. (mm)	Stroke (mm)	Packing material
1	25	10	300	Nitrile rubber
2	40	16	200	
3	63	20	200	

Experimental Results

Figure 4 shows the measured friction force-displacement characteristics at three conditions of the variation of the pressure p_1 at p_s=0.4 MPa and p_2=0 MPa in the extending stroke of Cylinder 1. In Figure 4a, when the pressure p_1 is gradually increased to p_{1max}=0.017 MPa, the piston moves to a new position of x=0.07mm from the original position. After that, when the pressure p_1 is gradually reduced to zero, the piston moves back to its original position following a new curve, and a hysteresis loop is created. This result presents an elastic movement of the piston. In Figure 4b, when the pressure p_1 is gradually increased to p_{1max}=0.025 MPa that is larger than that in Figure 4a and then gradually reduced to zero, the piston does not move back to its original position but stops at a new position of x=0.025 mm. When the same value of p_1 is re-applied, the same processes are repeated and the piston stops at new positions. This result shows that the movement of the piston includes both elastic and plastic movements. Essentially, the piston movement in pre-sliding regime obtained in Figures 4a and 4b is caused by the elastic

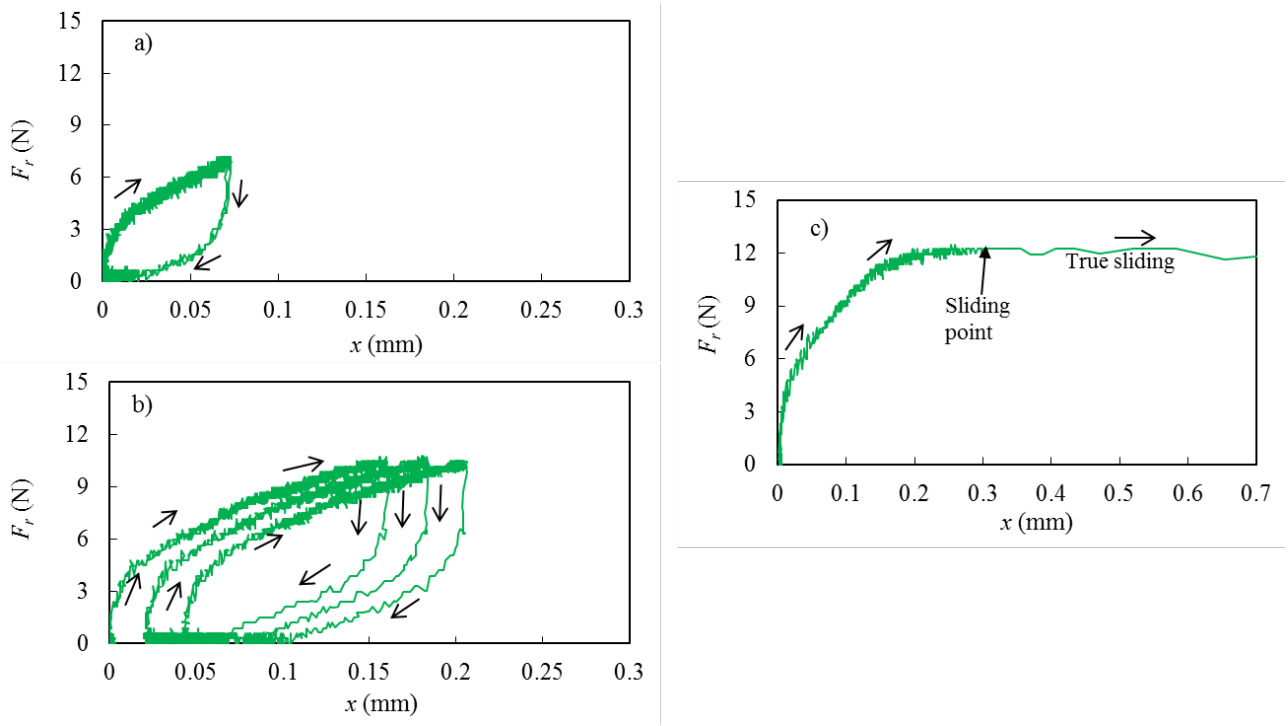

Figure 4. Friction force-displacement characteristics under different varying conditions of p_1 in the extending stroke of the piston at p_s=0.4 MPa and p_2=0 MPa (Cylinder 1): a) p_{1max}=0.017 MPa; b) p_{1max}=0.025 MPa; c) p_{1max}=0.028 MPa

and/or plastic deformations of the asperity junctions between the piston seal and cylinder wall and between the rod seal and rod surface. When the pressure p_1 is increased to a large enough value p_{1max}=0.028 MPa, the piston motion enters its sliding regime, as shown in Figure 4c. At the sliding point, the asperity junctions between the piston/rod seals and the

cylinder wall/rod surface are broken, and a sliding motion begins. It is noted that the piston velocity is nearly zero in the pre-sliding regime and suddenly increase from zero to a very high value when entering to the sliding regime as shown in Figure 5. Therefore, the sliding point is determined at the increasing point of the velocity.

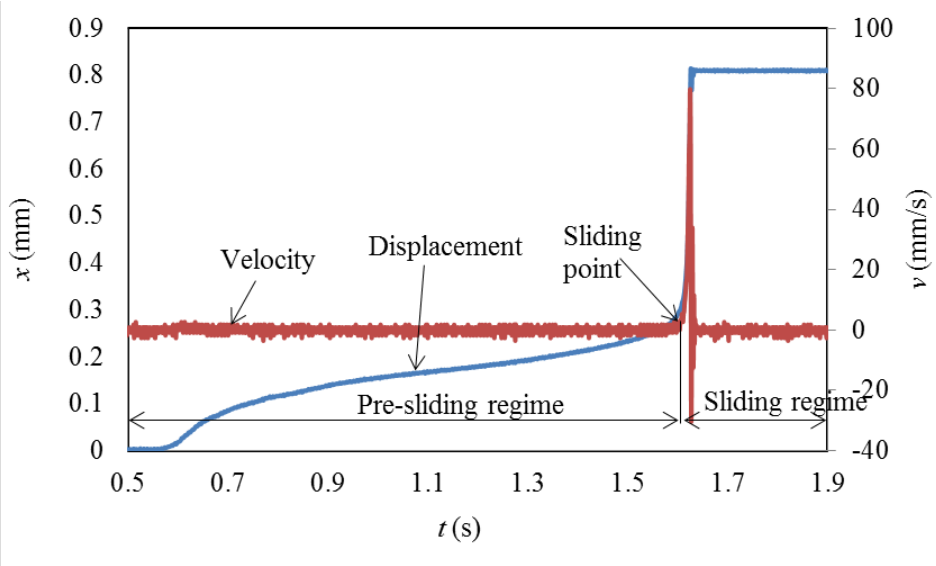

Figure 5. Experimental characteristics of piston displacement and velocity. The piston displacement is corresponded to Figure 4c.

The same behavior as that shown in Figure 4 can be observed for the retracting stroke of the piston for Cylinder 1 in Figure 6, where the pressure p_2 was varied between 0 and certain values and the pressure p_1 was kept at 0 MPa. Figures 7 and 8 show the measured friction force-displacement characteristics at different conditions of the variation of the pressure p_1 and p_2=0 MPa in the extending stroke of Cylinders 2 and 3, respectively. It can be seen from Figures 4, 6 to 8 that the shape of the friction force-displacement curves are different between the three cylinders but the effects of the pressure variation on the friction force-displacement curves are similar for three cylinders. In addition, it can be also realized that the friction behaviour of the pneumatic cylinders in pre-sliding regime are similar to those of a nonlinear spring.

Figure 9 shows an experimental result of the friction force-displacement characteristic of Cylinder 1, which is obtained when the pressure p_1 is gradually increased to a certain value under p_2=0 (segment 1), then is gradually decreased to zero (segment 2), and after that the pressure p_2 is gradually increased under p_1=0 (segment 3) and then gradually decreases to zero (segment 4). The supply pressure was kept constant at 0.4 MPa for this case. The result shows a clockwise hysteresis loop behaviour between the friction force and the displacement as shown in Figure 9c. Both elastic and plastic movements of the piston are included in the loop.

Figure 10 shows an experimental result of the friction force-displacement characteristic of Cylinder 1 obtained when the piston is slightly operated in extending or retracting stroke several times by increasing or decreasing either p_1 or p_2. Figure 10c shows that there are five small (internal) hysteresis loops in a large (external) hysteresis loop. The internal hysteresis loops are formed at different points on the external loop depending on the variation of the pressure p_1 or p_2. This behavior of friction can be also observed in other mechanisms [11, 12] and is called as hysteresis behavior with nonlocal memory [13]. A hysteresis behavior

with nonlocal memory is defined as an input–output relationship for which the output at any time instant depends not only on the output at some time instant in the past and the input since then, but also on past extremum values of the input or output [13]. Experimental results of the hysteresis behavior with nonlocal memories are also shown in Figure 11 for Cylinders 2 and 3.

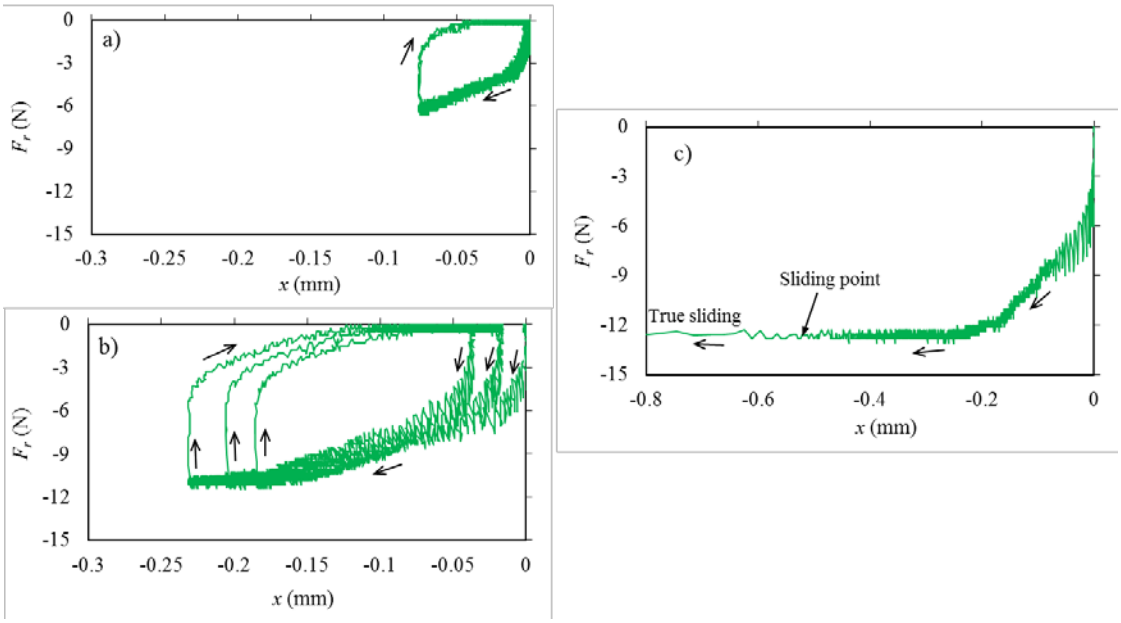

Figure 6. Friction force - displacement characteristics under different varying conditions of p_2 in the retracting stroke of the piston at p_s=0.4 MPa and p_1=0 MPa (Cylinder 1): a) p_{2max}=0.0186 MPa; b) p_{2max}=0.03 MPa; c) p_{2max}=0.034 MPa

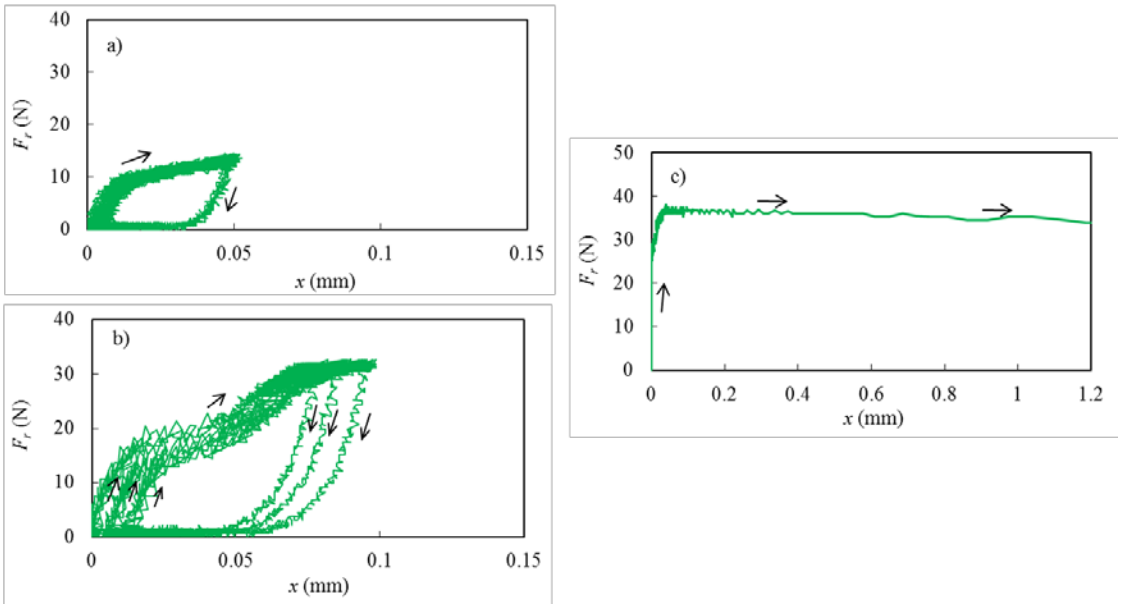

Figure 7. Friction force-displacement characteristics under different varying conditions of p_1 in the extending stroke of the piston at p_s=0.4 MPa and p_2=0 MPa (Cylinder 2): a) p_{1max}=0.01 MPa; b) p_{1max}=0.024 MPa; c) p_{1max}=0.0286 MPa

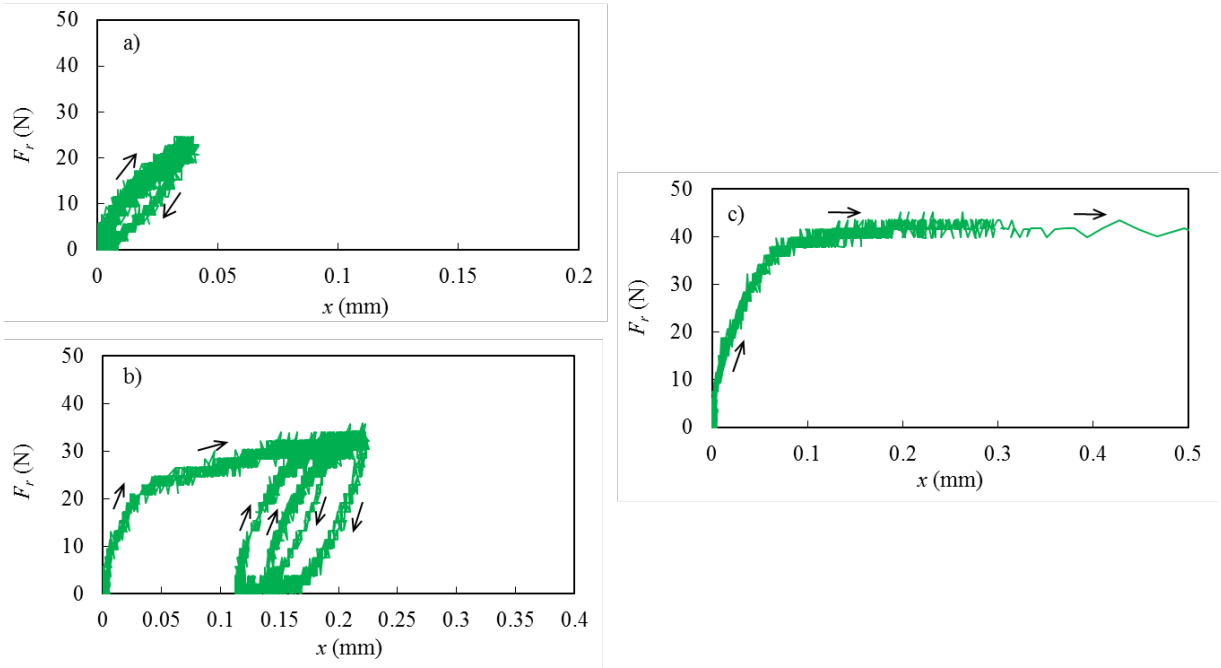

Figure 8. Friction force-displacement characteristics under different varying conditions of p_1 in the extending stroke of the piston at p_s=0.4 MPa and p_2=0 MPa (Cylinder 3): a) p_{1max}=0.008 MPa; b) p_{1max}=0.011 MPa; c) p_{1max}=0.013 MPa

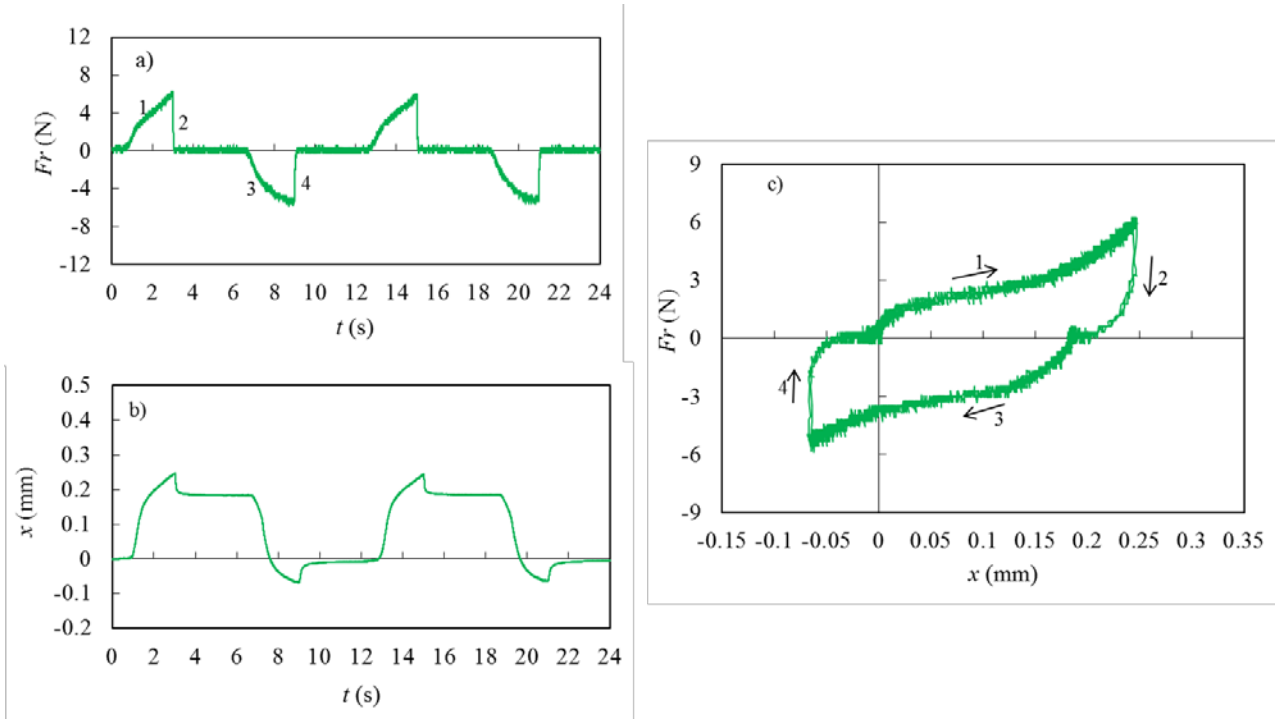

Figure 9. Friction force-displacement characteristic in both extending and retracting strokes (Cylinder 1): a) variation of friction force, b) variation of piston displacement, c) friction force versus displacement

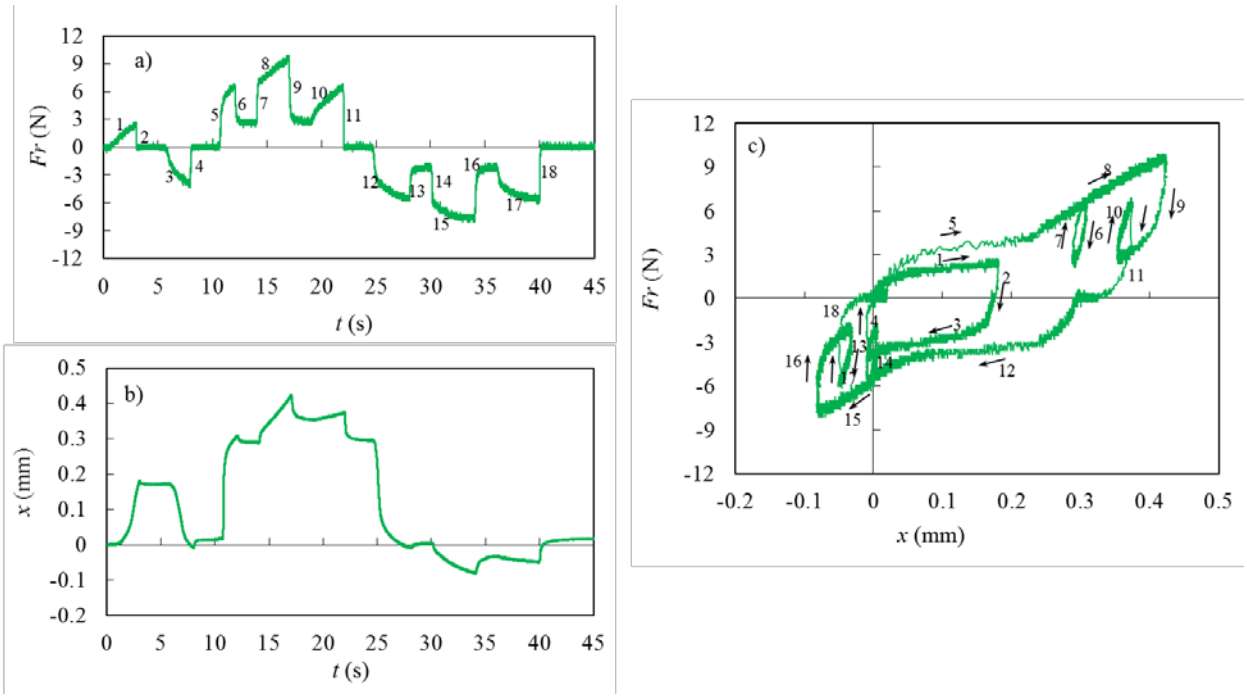

Figure 10. Hysteresis behavior observed in the friction force-displacement characteristic (Cylinder 1): a) variation of friction force, b) variation of piston displacement, c) friction force versus displacement.

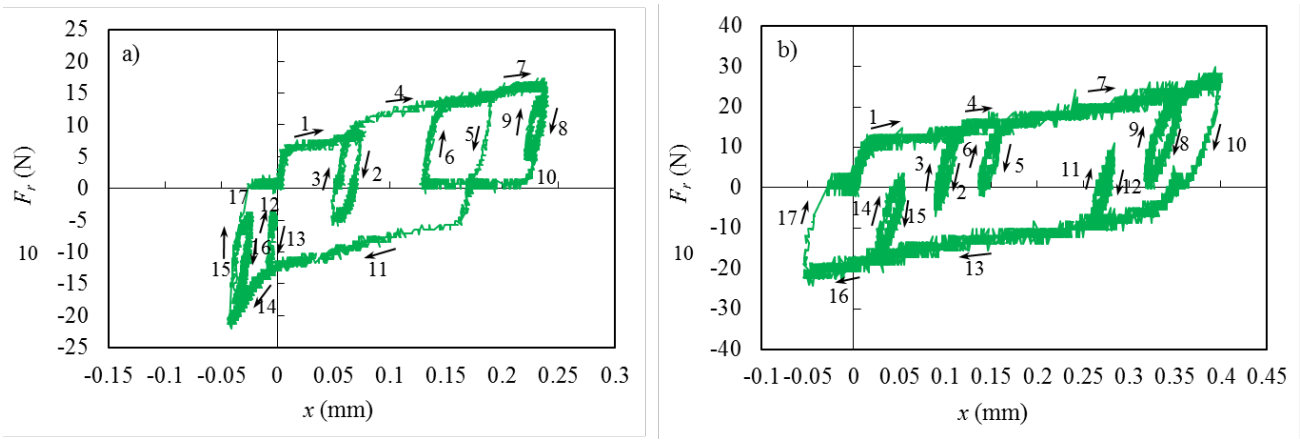

Figure 11. Experimental results of hysteresis behavior with nonlocal memory: a) Cylinder 2, b) Cylinder 3.

Figure 12 shows variations of the hysteresis loop when the pressures p_1 and p_2 are increased to different maximum values for Cylinder 1. In Figure 12a, p_1 is increased to three maximum values of 0.01, 0.014, and 0.02 MPa while p_2 is kept increasing to a maximum value of 0.016MPa, and in Figure 12b, p_2 is increased to three maximum values of 0.0095, 0.016, and 0.022 MPa while p_1 is kept increasing to a maximum value of 0.014MPa. Time periods of pressure variation are kept constant each condition. It is shown in Figure 12 that the loop size is increased with the increase in the pressure p_1 or p_2. However, the shape of the hysteretic loop is not affected by the magnitude of the pressure.

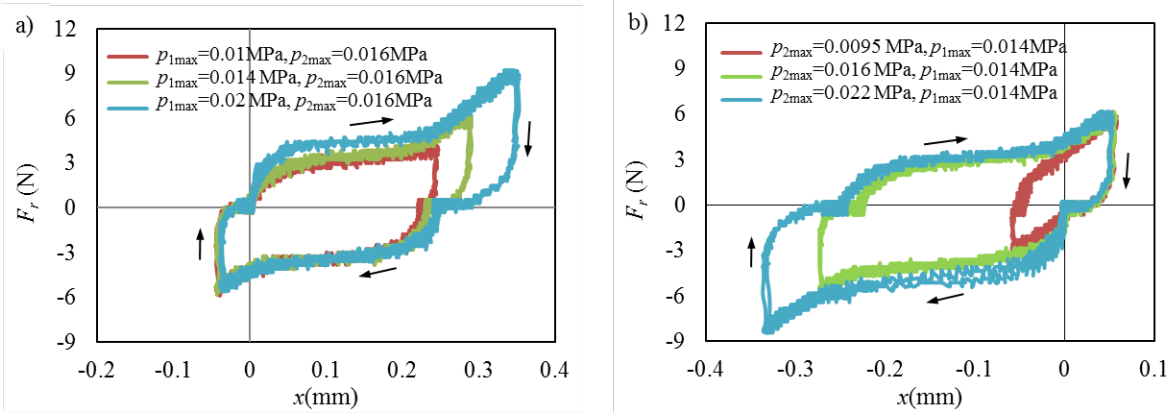

Figure 12. Effects of the pressures p_1 and p_2 on the hysteresis loop (Cylinder 1 at p_s =0.4 MPa): a) effect of p_1, b) effect of p_2.

Friction Model

New Modified LuGre Model

Tran et al. [8] have revised the modified LuGre model [6] for simulating the dynamic friction behavior of hydraulic cylinders by replacing the usual fluid friction term with a first-order lead dynamics. This model is called the new modified LuGre model (NMLGM). Similarly to the LuGre model, the NMLGM is based on the bristle model shown in Figure 13 in which contacting asperities on the surfaces are modeled as rigid bristles on one surface and elastic ones on another surface. z denotes the mean deflection of the elastic bristles and is modeled by

$$\frac{dz}{dt} = v - \frac{\sigma_0 z}{g(v,h)} v \tag{2}$$

where v is the velocity of the sliding surface, σ_0 is the stiffness of the bristles. $g(v,h)$ is a Stribeck function and is expressed by

$$g(v,\, h) = F_c + \left[(1-h)F_s - F_c\right] e^{-(v/v_s)^n} \tag{3}$$

where F_c is the Coulomb friction force, F_s is the maximum static friction force, v_s is the Stribeck velocity, n is an appropriate exponent. h is the dimensionless lubricant film thickness parameter and is described as

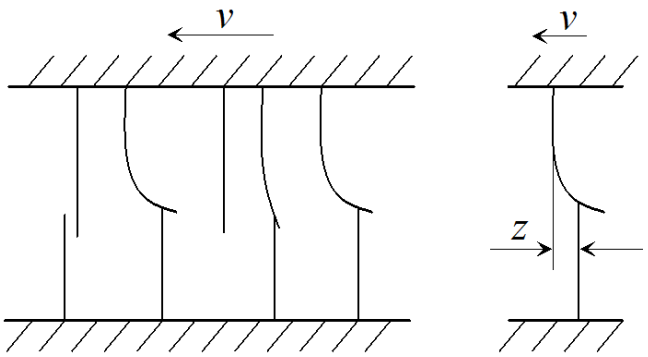

Figure 13. Bristle model

$$\frac{dh}{dt} = \frac{1}{\tau_h}(h_{ss} - h) \tag{4}$$

$$\tau_h = \begin{cases} \tau_{hp} & (v \neq 0,\ h \leq h_{ss}) \\ \tau_{hn} & (v \neq 0,\ h > h_{ss}) \\ \tau_{h0} & (v = 0) \end{cases} \tag{5}$$

$$h_{ss} = \begin{cases} K_f \,|v|^{2/3} & (|v| \leq |v_b|) \\ K_f \,|v_b|^{2/3} & (|v| > |v_b|) \end{cases} \tag{6}$$

$$K_f = (1 - F_c / F_s)|v_b|^{-2/3} \tag{7}$$

where h_{ss} is the dimensionless lubricant film thickness parameter in steady-state, τ_{hp}, τ_{hn}, τ_{h0} are the time constants for acceleration, deceleration, and dwell periods, respectively, K_f is the proportional constant, v_b is the maximum velocity for the lubricant film thickness variation.

The friction force F_r generating from the bending of the bristles and from the fluid friction is given by

$$F_r = \sigma_0 z + \sigma_1 \frac{dz}{dt} + \sigma_2 \left(v + T \frac{dv}{dt} \right) \tag{8}$$

where σ_1, σ_2 are the micro-viscous friction coefficient and the viscous friction coefficient, respectively, T is the time constant for fluid friction dynamics.

For steady-state, the friction force is described as follows

$$F_{rss} = F_c + [(1 - h_{ss})F_s - F_c]e^{-(v/v_s)^n} + \sigma_2 v \tag{9}$$

The new modified LuGre model can simulate well the friction behavior of the hydraulic and pneumatic cylinders observed in their sliding regime [9, 10]. However, as shown in Figure 14, the model is incapable to simulate the friction behavior in pre-sliding regime of a pneumatic cylinder measured using the experimental system proposed in this study. The parameters of the model used in the simulation are shown in Table 4 for Cylinder 1 in Section of Model Validation. The velocity calculated from the measured piston displacement in Figure 14a was used as the input to the model. When the piston displacement is varied as shown in Figure 14a, the friction force versus displacement curve exhibits a hysteresis behavior with nonlocal memories. There are an external hysteresis loop and two internal hysteresis loops within it (Figure 14c). It can be seen in Figure 14c that the measured hysteresis behavior with nonlocal memories cannot be accounted by NMLGM; the magnitude of the friction force and the shape of the hysteresis loop obtained by the model are clearly different from those of the experimental result. It is noted that the contribution of the second and third terms in Equation (8) to friction force is negligible in pre-sliding regime. Therefore, the friction force mainly depends on the first term $\sigma_0 z$. Only the parameter σ_0 that represents the stiffness of elastic bristles determines the magnitude of the friction force and the shape of the hysteresis loop. The new modified LuGre model is therefore inadequate for simulating the measured friction behavior of the pneumatic cylinder in pre-sliding regime.

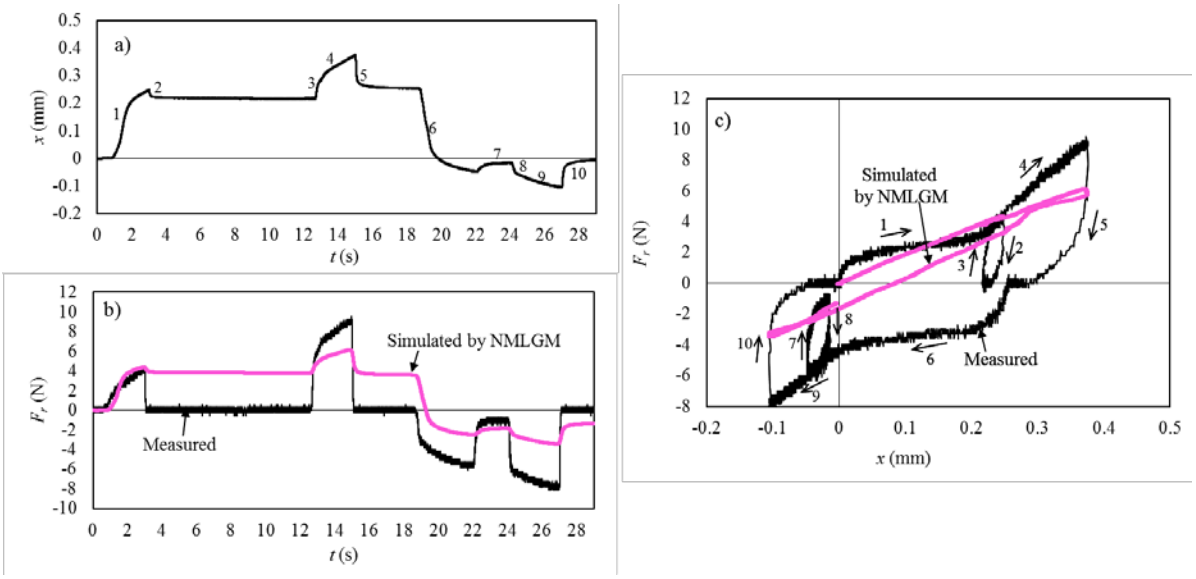

Figure 14. Friction force –displacement characteristics measured by the proposed experimental setup in pre-sliding regime of Cylinder 1 and simulated by the new modified LuGre model (NMLGM).

New Model

As mentioned above, the new modified LuGre model is based on the LuGre model. Swevers et al. [14] have shown that the LuGre model itself has a drawback in expressing friction behavior in pre-sliding regime. In order to overcome this drawback, they have proposed the Leuven model, which replaces the friction force term $\sigma_0 z$ with a function $F(z)$ that exhibits the hysteresis behavior with nonlocal memory. However, the Leuven model is complicated and its programming is not easy. Taking these into account, a new friction model is proposed for pneumatic cylinders by modifying the new modified LuGre model as follows:

$$\frac{dz}{dt} = v - \frac{F(z)}{g(v,h)}v \tag{10}$$

$$F_r = F(z) + \sigma_1 \frac{dz}{dt} + \sigma_2\left(v + T\frac{dv}{dt}\right) \tag{11}$$

$$F(z) = \begin{cases} \sigma_0 z & \text{for } |z| \geq |F_s|/\sigma_0 \\ f_i(z) \quad (i = 1, 2, \cdots) & \text{for } |z| < |F_s|/\sigma_0 \end{cases} \tag{12}$$

where $f_i(z)$ (i=1,2, …) are the functions that model segments of transition curve and i is the segment name. The friction force-deflection curve in pre-sliding regime consists of transition curves, i.e. curves between two velocity reversal points. Each velocity reversal starts a new transition curve and each transition curve can be divided into some segments depending on its shape. Experimental results later showed that each segment can be approximated by a function $f_i(z)$ as follows:

$$f_i(z) = f_i(z_i) + c_i\left(1 - e^{-k_i(z-z_i)}\right) \quad \text{or} \quad \frac{df_i}{dz} = c_i k_i e^{-k_i(z-z_i)} \tag{13}$$

where c_i and k_i are the segment parameters that can be identified from experimental friction force-displacement characteristics, $c_i k_i$ indicates the stiffness of the bristles at $z=z_i$, z_i is the initial deflection on the i-th segment, and $f_i(z_i)$ is the initial friction force of the i-th segment and equals to the final friction force of the (i-1)-th segment.

Implementation of the function $F(z)$ in pre-sliding regime of the proposed model requires two memory sets for the functions $f_i(z)$: one for ascending curves ($v>0$) and one for descending curves ($v<0$). The sets begin at velocity reversal and remove when a hysteresis loop is closed. At each inverse point of velocity, the deflection z takes a maximum value z_m (see Figure 15a) or a minimum value z_n (see Figure 15b). At these points, a new transition curve begins and the function $f_{i+1}(z)$ is calculated by resetting z_i in Equation (13) to z_m or z_n and $f_i(z_i)$ will take the value F_m or F_n, respectively.

For an internal loop, it is shown in Figures 10 and 11 that when an internal hysteresis loop is closed, the loop is removed from the memory and has no influence on the future curve. Figure 16 illustrates internal loops created on an ascending curve (Figure 16a) and on a descending curve of external loop (Figure 16b). The internal loop is formed by two curves 2 and 3 between two velocity reversal points at z_n and z_m. When the velocity reverses at z_n, the numerical program will judge the state to be on the internal loop by checking the variation of velocity sign from positive to negative. The state is calculated by a function $f_{i+1}(z)$ using the parameters c_{i+1}, k_{i+1} and the values of z_n and F_n. When the velocity reverses at z_m, the numerical program will remain the state on the internal loop and the state is calculated by a function $f_{i+2}(z)$ using the parameters c_{i+2}, k_{i+2} and the values of z_m and F_m. After the velocity reversal point z_m, a function $f_i(z)$ of the curve 1 on the external loop is calculated together with the function $f_{i+2}(z)$ of the curve 3. When the value

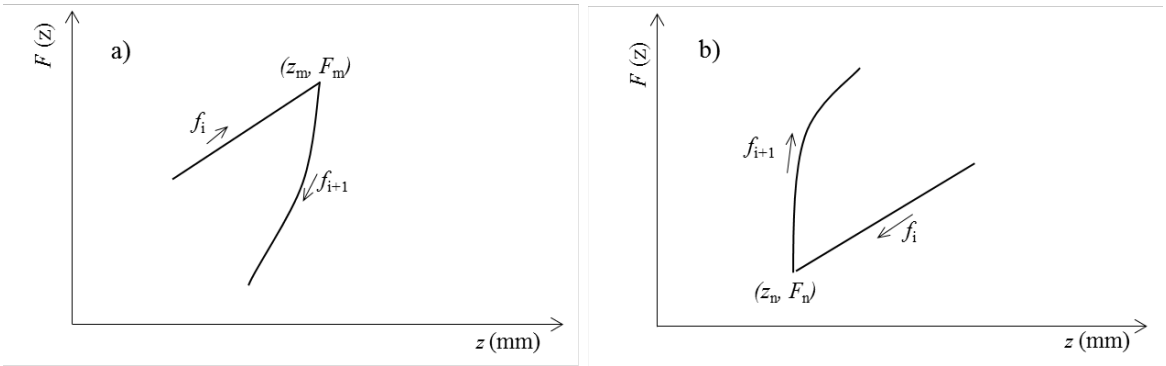

Figure 15. Numerical implementation of the function $f_i(z)$ at motion reversal.

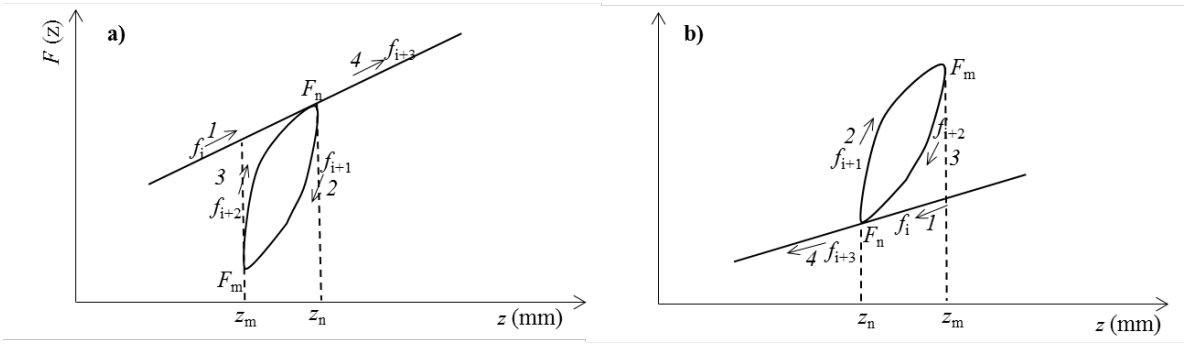

Figure 16. Numerical implementation of internal hysteresis loop: a) internal loop on an ascending external curve, b) internal loop on a descending external curve

of $f_{i+2}(z)$ reaches the value of $f_i(z)$ at the point in the vicinity of z_n and when there is no change in velocity sign, the friction state has to follow the curve 1 or curve 4 on the external loop after the intersection point z_n. The values of z_n, F_n, z_m and F_m of the internal loop are automatically cleared from the program after the intersection point z_n.

When the piston movement enters its sliding regime, i.e., when the deflection reaches F_s/σ_0, the model is then switched to the new modified LuGre model. At this condition, the hysteresis function $F(z)$ is set equally to $\sigma_0 z$.

Identification of *f*(*z*)

The functions $f_i(z)$ can be identified from the experimental friction force-displacement characteristics. Figure 17 shows an external hysteresis loop obtained by experiment for Cylinder 1. The external hysteresis loop includes an ascending transition curve (v>0) and a descending transition curve (v<0). The ascending curve in this case can be divided into three segments corresponding to the following deflection ranges of the bristles: [$-z_1$, 0], [0, z_3] and [z_3, z_5], and the descending curve can be divided into three segments corresponding to the following deflection ranges of the bristles: [$-z_1$, z_2], [z_2, z_4] and [z_4, z_5]. The values of z_1, z_2, z_3, z_4 and z_5 are shown in Table 2. The three segments on the ascending curve can be approximated by three exponential functions $f_1(z)$, $f_2(z)$, and $f_3(z)$, and the three segments on the descending curve can be approximated by three exponential functions $f_4(z)$, $f_5(z)$, and $f_6(z)$ given by Equation (13).

When the pressure variation is increased, size of the transition curve is expanded as shown in Figure 12 and, therefore, the values of z_1 and z_5 can be expanded to maximum deflections at which the piston moves from pre-sliding regime to sliding regime. However, the value of z_2, z_3, z_4 and shape of the curves in six ranges are unchanged with the pressure variations. Therefore, the six deflection ranges of the external loop can be approximated by Equation (13) by assigning appropriate values to c_i and k_i (i=1 to 6). It can be seen from Figure 17, the descending curve is almost inversely symmetrical with the ascending curve. Therefore, the values of c_i and k_i (i=4 to 6) can be set equally to the minus values of c_i and k_i (i=1 to 3) respectively.

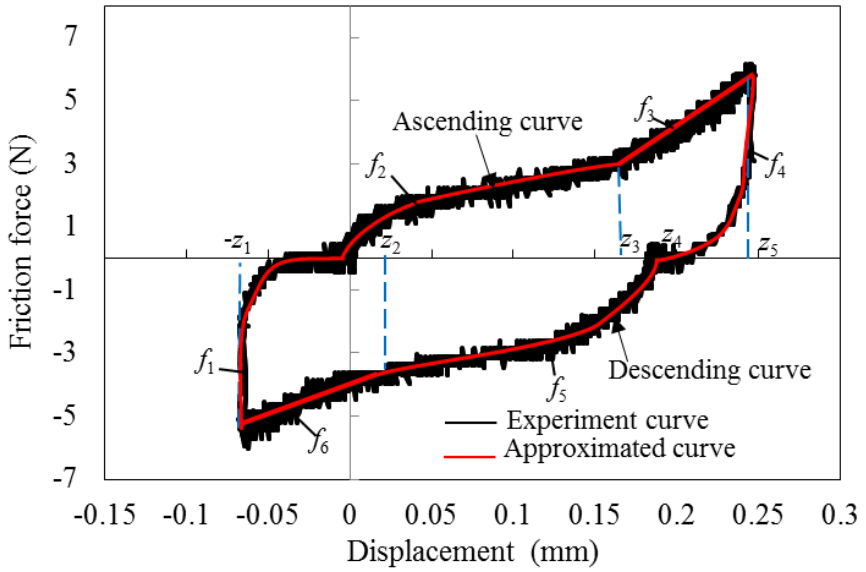

Figure 17. Identification of hysteresis functions $f_i(z)$ from the measured friction force – displacement curve (external loop).

Table 2. Values of the Deflection z_i (i=1 to 5) in Figure 15

Parameter	z_1 (mm)	z_2 (mm)	z_3 (mm)	z_4 (mm)	z_5 (mm)
Value	1.25×10^{-4}	0.84×10^{-4}	1.59×10^{-4}	1.78×10^{-4}	2.29×10^{-4}

Figure 18 shows an example of the internal hysteresis loop obtained by experiment. The internal hysteresis loop also includes an ascending transition curve ($v>0$) and a descending transition curve ($v<0$) in a deflection range between $z_c = 2.46\times10^{-4}$ mm and $z_d = 2.65\times10^{-4}$ mm. These values of z_c and z_d are determined at corresponding displacement points of 0.292 mm and 0.311 mm respectively by simulation. The descending curve can be approximated by only a function $f_7(z)$ and the ascending curve can be approximated by only a function $f_8(z)$ in Equation (13). It can be also seen from Figure 18 that the descending curve is almost inversely symmetrical with the ascending curve. Therefore, the values of c_7 and k_7 can be set equally to the minus values of c_8 and k_8 respectively.

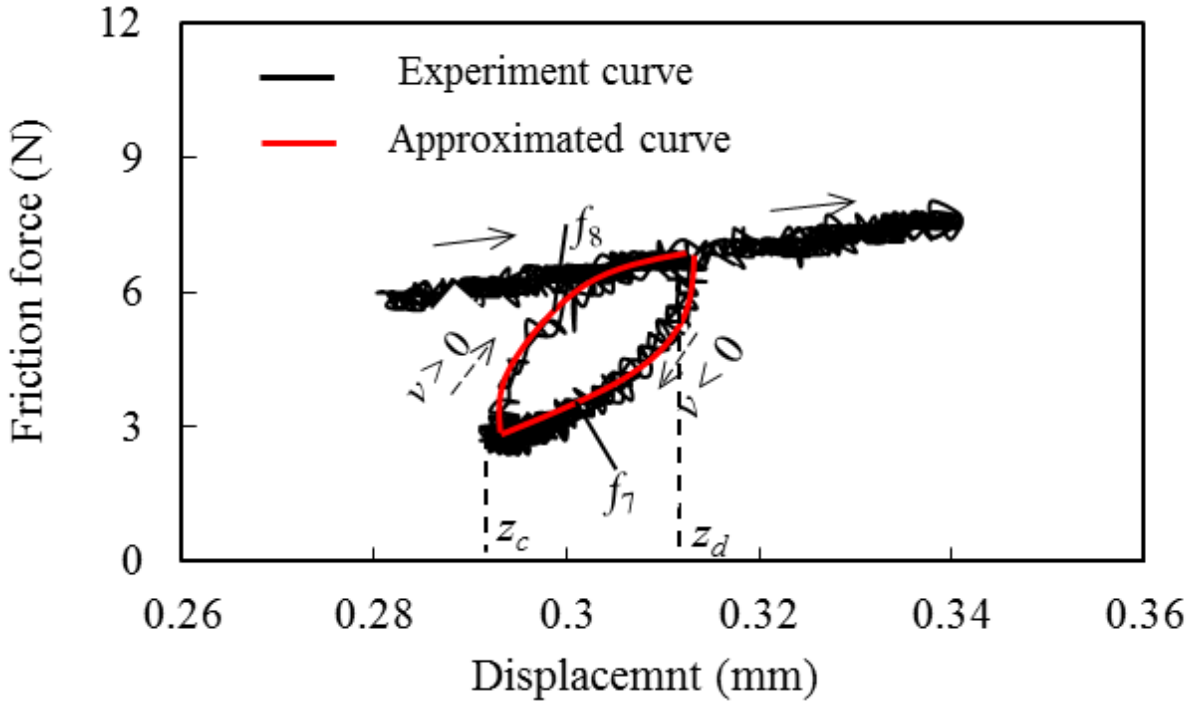

Figure 18. Identification of hysteresis function $f_i(z)$ from the measured friction force-displacement curve (internal loop)

The parameters c_i and k_i (i=1 to 3, 8) are identified by fitting Equation (13) to the measured segments. Table 3 shows the identified values of the parameters c_i and k_i for the measured friction force - displacement curves in Figures 17 and 18. The identified parameters c_i and k_i are almost the same for internal loops at various points of the bristle deflection. Therefore, any friction characteristic in the pre-sliding regime can be approximately expressed by the four sets of the parameters shown in Table 3.

Table 3. Examples of the Identified Parameters of the Hysteresis Function $f_i(z)$ for Cylinder 1

	Parameter	Value [N]	Parameter	Value [m^{-1}]
External loop in Fig. 17	c_1	2	k_1	3×10^5
	c_2	1.7	k_2	3×10^4
	c_3	1.8	k_3	3.4×10^5
Internal loop in Fig. 18	c_8	4.05	k_8	1.8×10^5

By incorporating the hysteresis functions $f_i(z)$ into the new friction model, additional parameters are introduced. The number of the parameters depends on how accurately measured transition curves are approximated and how complex those curves are.

Validation of Friction Model

In this section, the new friction model is validated using the results measured in the three pneumatic cylinders. Simulation was done using MATLAB/Simulink. Velocity wave forms calculated from the measured piston displacement signals were used as the input to the model. The parameters of the new friction model F_s, F_c, v_s, v_b, n, σ_0, σ_1, σ_2, τ_{hp}, τ_{hn}, τ_{h0}, and T used in simulation are shown in Table 4. These parameters were taken from Tables 2 and 3 in [10] of Standard cylinder (Cylinder 1 in this study) at p_1=0.3 MPa and p_2=0 MPa in extending stroke and at p_1=0 MPa and p_2=0.3 MPa in retracting stroke of the cylinder at frequency of the velocity variation f=0.5 Hz, and were determined by trial and error for Cylinders 2 and 3. It is shown in [10] that some parameters of NMLGM such as F_s, F_c and v_s are affected by the pressures p_1 and p_2. However, in this study, the variation of the pressures in pre-sliding regime is relatively small and, therefore, the effects of the variations of F_s, F_c and v_s on the simulation results are negligible. The variation of the parameters v_b, v_s, F_c, and σ_2 with the frequency is determined by Equation (12) in [10]. The parameters of the hysteresis function c_i and k_i of the new friction model were identified experimentally by the method proposed above.

Table 4. Values of the Parameters of the New Friction Model Used in Simulation for Three Pneumatic Cylinders

Parameters	Cylinder 1		Cylinder 2		Cylinder 3	
	$v > 0$	$v < 0$	$v > 0$	$v < 0$	$v > 0$	$v < 0$
F_s [N]	22.5	-25	25	-27	32	-28.5
F_c [N]	5.5	-5.8	6.2	-6	7.3	-6.8
v_s [m/s]	0.01	-0.055	0.07	-0.07	0.045	-0.052
v_b [m/s]	0.037	-0.025	0.037	-0.025	0.037	-0.025
n	2.5	1.2	2.5	2.5	2.7	2.8
σ_2 [Ns/m]	25	25	26	26	30	30
σ_0 [N/m]	1.5×10^4		1.62×10^4		1.8×10^4	
σ_1 [Ns/m]	0.1		0.1		0.1	
τ_{hp} [s]	0.02		0.012		0.025	
τ_{hn} [s]	0.15		0.14		0.12	
τ_{h0} [s]	20		22		25	
T [s]	0		0		0	

Figure 19 shows comparisons of the friction force-displacement characteristic between simulation and experiment for three pneumatic cylinders. The comparison results show that the external and internal hysteresis curves simulated by the new friction model agree relatively well with the measured curves. A comparison of the measured friction characteristic in time series and that simulated by the new model is shown in Figure 20. It shows that the simulation curves follow well the measurement curves. Figure 21 shows comparisons of the friction force-velocity characteristics between simulation by the new model and experiment in the sliding regime. The experimental results were taken from Figure 8a in [10] in the extending stroke of the Standand cylinder (Cylinder 1) at two frequencies of 0.5 Hz and 2 Hz. Figure 21 show that the new friction model can also give good simulation results of the friction behavior of the pneumatic cylinder in the sliding regime.

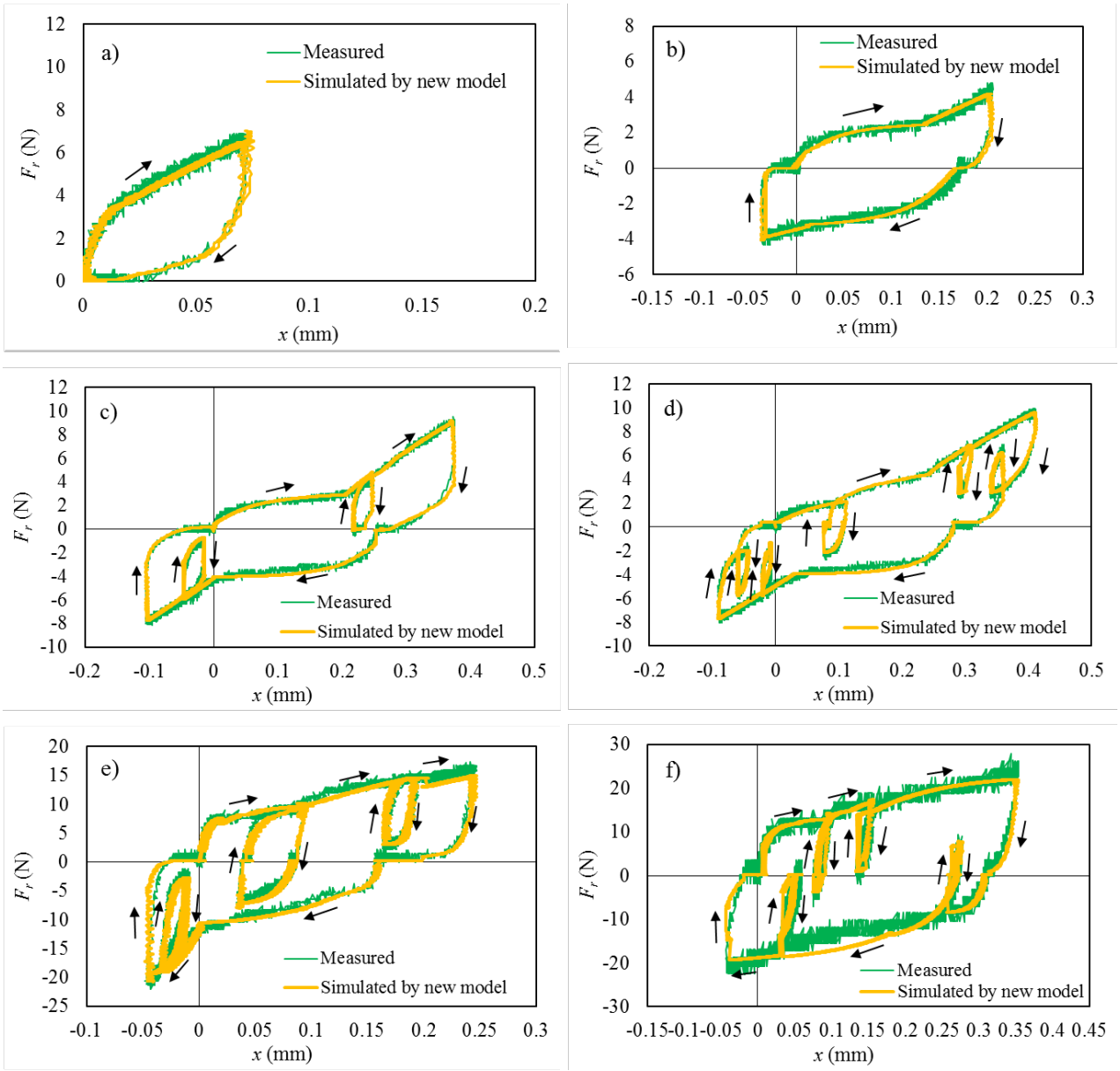

Figure 19. Comparison between measured friction force-displacement characteristics and those simulated using the new friction model: a-d) Cylinder 1 at P_s=0.4 MPa; e) Cylinder 2 at P_s=0.5 MPa; f) Cylinder 3 at P_s=0.5 MPa.

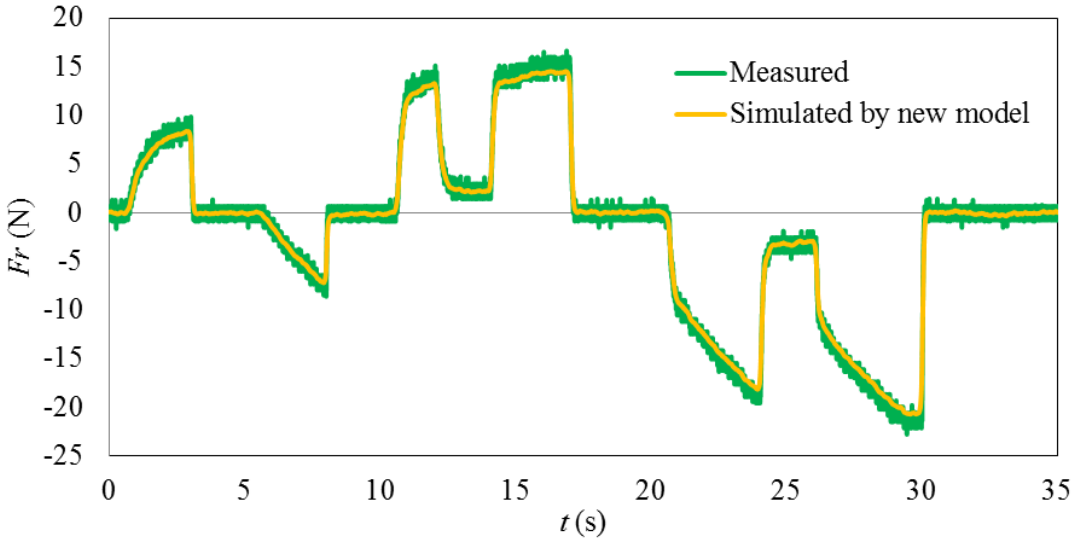

Figure 20. Comparison between measured friction force characteristic and that simulated using the new friction model for Cylinder 2 at P_s=0.5 MPa.

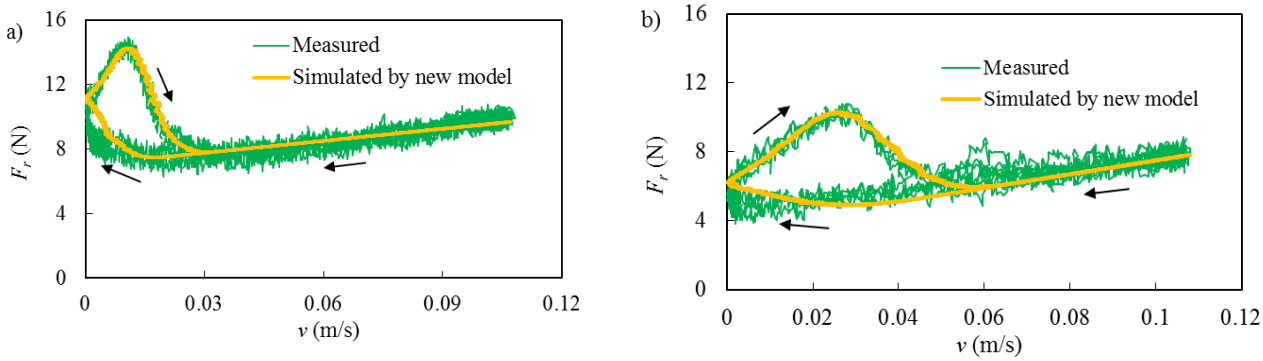

Figure 21. Comparison between friction force-velocity characteristics measured in true sliding regime by the experimental setup presented in [10] and those simulated using the new friction model at different frequencies of velocity variation: a) f=0.5Hz, b) f=2Hz

Conclusions

In this paper, dynamic friction behavior of pneumatic cylinders in pre-sliding regime is investigated using an experimental setup. In addition, a new friction model that can express friction behavior in both sliding and pre-sliding regimes is proposed by incorporating hysteresis functions into the new modified LuGre model. The following conclusions can be drawn from this study:

i) Friction behavior in pre-sliding regime is represented by the behavior of a nonlinear spring.
ii) Hysteresis behavior with nonlocal memory is observed when the velocity is reversed.
iii) Size of the hysteresis loop is increased by increasing the pressures in the cylinder chambers.
iv) The new friction model can simulate well all the observed friction behavior in both pre-sliding and sliding regimes.

Applications of the new friction model to the simulation of the dynamic behavior of pneumatic cylinder systems will be the subject for a future study.

Acknowledgement

This research was funded by Collaborative Research Program for Alumni Members (CRA), AUN/SEED-Net, JICA under grant numbers HUST CRA 1401 and HUST CRA 1501.

References

[1] A. Hibi, and T. Ichikawa, "Mathematical model of the torque characteristics for hydraulic motors," *Bulletin of JSME*, Vol. 20, No.143, pp. 616–21, 1977.

[2] L.E. Schroeder, and R. Sigh, "Experimental study of friction in a pneumatic actuator at constant velocity," *Journal of Dynamic Systems, Measurement, and Control*, Vol. 115, No. 3, pp. 575-577, 1993.

[3] G. Belforte, G. Mattiazzo, and S. Mauro, "Measurement of friction force in pneumatic cylinders," *Tribotest Journal*, Vol. 10, No. 1, pp. 33-48, *2003*.

[4] P.L. Andrighetto, A.C. Valdiero, and L. Carlotto, "Study of the friction behavior in industrial pneumatic actuators," *ABCM Symposium Series in Mechatronics*, Vol. 2, pp. 369 – 376, 2006.

[5] B.M.Y. Nouri, "Friction identification in mechatronic systems," *ISA Transactions, Vol.* 43, pp. 205–216, 2004.

[6] H. Yanada, and Y. Sekikawa, "Modeling of dynamic behaviors of friction," *Mechatronics*, Vol. 18, No. 7, pp. 330-339, 2008.

[7] C.C. de Wit, H. Olsson, K.J. Astrom, and P. Linschinsky, "A new model for control of systems with friction," *IEEE Transactions Automatic Control*, Vol. 40, No. 3, pp. 419–425, 1995.

[8] X.B. Tran, A. Matsui, and H. Yanada, "Effects of viscosity and type of oil on dynamic behaviors of friction of hydraulic cylinder," *Transactions of the Japan Fluid Power System Society*, Vol. 41, No. 2, pp. 28–35, 2010.

[9] X.B. Tran, N. Hafizah, and H. Yanada, "Modeling of dynamic friction behaviors of hydraulic cylinders," *Mechatronics*, Vol. 22, No.1, pp. 65-75, 2012.

[10] X.B. Tran, and H. Yanada, "Dynamic friction behaviors of pneumatic cylinders," *Intelligent Control and Automation*, Vol. 4, No.2, pp. 180-190, 2013.

[11] V. Lampaert, F. Al-Bender and J. Swevers, "Experimental characterization of dry friction at low velocities on a developed tribometer setup for macroscopic measurements," *Tribology Letters*, Vol. 16, No. 1, pp. 95-105, 2004.

[12] K. DeMoerlooze and F. Al-Bender, "Experimental investigation into the tractive prerolling behavior of balls in v-grooved tracks," *Advances in Tribology*, Vol. 2008, pp. 1-10, 2008.

[13] I.D. Mayergoyz, *Mathematical Models of Hysteresis*. Springer Verlag, New York, 1991.

[14] J. Swevers, F. A. Bender, C.G. Ganseman, and T. Prajogo, "An integrated friction model structure with improved presliding behavior for accurate friction compensation," *IEEE Transactions on Automatic Control*, Vol. 45, No. 4, pp. 675-686, 2000.